PROCEEDINGS OF SCIENCE

Constraints on sterile neutrino mixing using IceCube atmospheric neutrino data

Soebur Razzaque*
Centre for Astro-Particle Physics (CAPP) and Department of Physics, University of Johannesburg, P.O. Box 524, Auckland Park 2006, South Africa
E-mail: srazzaque@uj.ac.za

Luis Salvador Miranda
Centre for Astro-Particle Physics (CAPP) and Department of Physics, University of Johannesburg, P.O. Box 524, Auckland Park 2006, South Africa
E-mail: smiranda-palacios@uj.ac.za

Sterile neutrinos with ~ 1 eV mass scale can resolve anomalies reported in short-baseline neutrino oscillation experiments. The same sterile neutrinos can affect the atmospheric neutrino fluxes at the detectors such as IceCube in the TeV energy range. Recent IceCube search results for a sterile neutrino resulted in stringent constraints on its mass and mixing with active neutrinos, essentially excluding the parameter space favored by the short-baseline experiments. In our recent reanalysis of IceCube data we show that sterile-active neutrino mixing schemes affect interpretation of the excluded parameter regions. We present exclusion regions in the mixing angle range $0.01 \leq \sin^2\theta_{24} \leq 0.1$ and mass-squared difference range $0.1\ \text{eV}^2 \leq \Delta m^2_{42} \leq 10\ \text{eV}^2$ for the mass-mixing and flavor-mixing schemes. We exclude the parameter space favored by recent MiniBooNE analysis at $\gtrsim 2\sigma$ CL for both schemes. Furthermore, we find that a prompt atmospheric neutrino flux contribution can relax the constraints on the sterile neutrino mass-squared difference for $\Delta m^2_{42} \gtrsim 1\ \text{eV}^2$.

36th International Cosmic Ray Conference -ICRC2019-
July 24th - August 1st, 2019
Madison, WI, U.S.A.

*Speaker.

PoS(ICRC2019)987

1. Introduction

Sterile neutrino mixing with the active neutrinos is one of the main research areas in neutrino physics. The anomalies reported by the short-baseline experiments such as the LSND [1] and MiniBooNE [2] can be explained using mixing of ~ 1 eV scale sterile neutrino(s). Furthermore, anomalies reported by the reactor [3, 4] and Gallium experiments [5] can not be explained within the standard 3-ν oscillation framework. More recently, several experiments have searched for sterile neutrinos [6, 7, 8, 9, 10, 11]. In particular, the recent IceCube and MINOS results show a strong tension between the appearance and disappearance experiments. IceCube reported a search for the disappearance results, excluding the allowed region of the appearance experiments, including those by the LSND and MiniBooNE, at 99% CL [12]. On the other hand, the latest MiniBooNE data combined with the LSND data result in a 6.0σ evidence of sterile neutrino [13].

In the case of long-baseline experiments, sterile neutrinos propagating through the earth's interior experience the matter effect and MSW or parametric resonance affecting the oscillation pattern [14, 15, 16, 17, 18, 19, 20]. In particular, an enhancement of the $\nu_\mu - \nu_s$ oscillations causes a reduction in the muon neutrino flux and distortion of the energy and zenith angle distributions of the atmospheric neutrino events in a detector such as the IceCube. Recent IceCube results considered the conventional atmospheric flux component only [12], although the flux data extend to $\sim 10^6$ GeV. The prompt component of the atmospheric flux, however, is important at energies $\gtrsim 10^5$ GeV and needs to be considered in the analysis to search for sterile neutrinos. Moreover, any constraints on the ν_s mixing parameters depend on the active-sterile mixing scheme. We addressed these issues in [20] using a prompt atmospheric flux model [21] as well as two mixing schemes for a 3+1 sterile-active mixing in [16]. In this proceedings, we present results published in [20].

2. Sterile neutrino mass- and flavor-mixing schemes

We consider mixing of the flavor states ν_f, including ν_s, with the mass states $\nu_{\rm mass}$ by the relation $\nu_f = U_f \nu_{\rm mass}$. The form of the unitary matrix U_f depends on the mixing schemes [16]. In the mass-mixing scheme ν_s mixes with a linear combination of the ν_3 and ν_4, and the mixing matrix is given by [20],

$$U_f = \begin{pmatrix} \cos\theta_{23} & -\sin\theta_{23}\cos\alpha & \sin\theta_{23}\sin\alpha \\ \sin\theta_{23} & \cos\theta_{23}\cos\alpha & -\cos\theta_{23}\sin\alpha \\ 0 & \sin\alpha & \cos\alpha \end{pmatrix} . \tag{2.1}$$

Here α is the mixing angle between ν_s and the linear combinations of ν_3 and ν_4. Note that for $\sin^2\theta_{23} = 1/2$, the elements $U_{\mu 4}$ and $U_{\tau 4}$ are equal. The relation between α and general rotation angles of eq. (2.1) satisfies the conditions:

$$\cos\alpha = \cos\theta_{24}\cos\theta_{34} \ , \ \sin\theta_{24} = \sin\theta_{34}/\cos\theta_{34}. \tag{2.2}$$

The matrix element that affects ν_μ is $U_{\mu 4} = \sin\theta_{23}\sin\alpha$ and the mixing is governed by the angle

α. The mixing matrix for the flavor-mixing scheme is given by [20]

$$U_f = \begin{pmatrix} \cos\theta_{24}\cos\theta_{23} & -\cos\theta_{24}\sin\theta_{23} & -\sin\theta_{24} \\ \sin\theta_{23} & \cos\theta_{23} & 0 \\ \sin\theta_{24}\cos\theta_{23} & -\sin\theta_{23}\sin\theta_{24} & \cos\theta_{24} \end{pmatrix}. \tag{2.3}$$

In this case ν_s does not mix with ν_4 since $U_{\tau 4} = 0$. The relevant matrix element in this scheme is $U_{\mu 4} = -\sin\theta_{24}$, with mixing angle θ_{24}. The relationship between θ_{24} and α in case of $\sin^2\theta_{23} = 1/2$ is $\sin^2\theta_{24} = \sin^2\alpha/(2-\sin^2\alpha)$.

2.1 Oscillation probabilities for $\bar{\nu}_\mu$ and ν_μ

In order to calculate the oscillation probabilities between the flavor states, we solve numerically the evolution equation $H_f = U_f M U_f^T/2E + V_f$. Here $M = \mathrm{diag}(m_2^2, m_3^2, m_4^2)$ and the potential matrix in the flavor base is $V_f = \mathrm{diag}(0, 0, -V_\mu)$, where we have subtracted the matrix $V_\mu I$ proportional to the identity matrix I. We assume normal mass hierarchy with $\Delta m^2_{32} = 2.5\times10^{-3}$ eV^2 and $\sin^2\theta_{23} = 1/2$, which are consistent with current experimental results [22, 23, 24]. The matter potential is given by $V_\mu = -G_F\rho/2\sqrt{2}m_N \approx -1.78\times10^{-14}\,(\rho/\mathrm{g/cc})$ eV, where ρ is matter density calculated from the density profile of the earth according to the Preliminary Reference Earth Model [25].

The search for sterile neutrinos for long baseline experiments such as IceCube takes place in the $\nu_\mu + \bar{\nu}_\mu$ channels using atmospheric fluxes. Note that the MSW resonance effect due to ν_s mixing occurs in the $\bar{\nu}_\mu$ channel, rather than in the ν_μ channel, because the matter potential is negative in this case. The oscillation probabilities for $\bar{\nu}_\mu$ (left panels) and ν_μ (right panels) are plotted in Figures 1 and 2, respectively, for the mass- and flavor-mixing schemes. The MSW resonance dips/peaks for the earth's mantle crossing trajectories with $\cos\theta_z = -0.6$, are located at the energy $E \propto \Delta m^2_{42}/2V_\mu$, a few TeV, for ~ 1 eV scale sterile neutrino. For the earth's core-crossing trajectories, shown in $\cos\theta_z = -1$ plots, the dips/peaks are due to parametric resonances. The relationship for muon neutrino survival probabilities between the two mixing schemes is given by $P^{(f)}_{\mu\mu} = (2\sqrt{P^{(\mathrm{mass})}_{\mu\mu}} - 1)^2$ [16].

3. Atmospheric fluxes and IceCube data

Atmospheric neutrino fluxes serve as natural beams to search for sterile neutrinos, mixing of which with the active neutrinos depletes the $\bar{\nu}_\mu$ fluxes at the detector after propagation through the earth. We use the Gaisser-Honda flux model for the conventional component [26, 27, 28] extended to PeV neutrinos [29] and the Enberg-Reno-Sarcevic flux model for the prompt component [21]. Figure 3 shows the fluxes without ν_s mixing (the total represented with a black solid line) as well as the fluxes with ν_s mixing, calculated as

$$\phi_\mu = \phi^0_\mu P_{\mu\mu} + \phi^0_e P_{e\mu} \approx \phi^0_\mu P_{\mu\mu}\,. \tag{3.1}$$

Here ϕ^0_μ and ϕ^0_e are the primary (un-oscillated) fluxes of atmospheric muon and electron neutrinos, respectively. The last approximation follows from the facts that $\phi^0_\mu \gg \phi^0_e$ and $P_{e\mu} \ll 1$. The fluxes affected by ν_s mixing are also shown in figure 3 with blue (mass-mixing) and red (flavor-mixing)

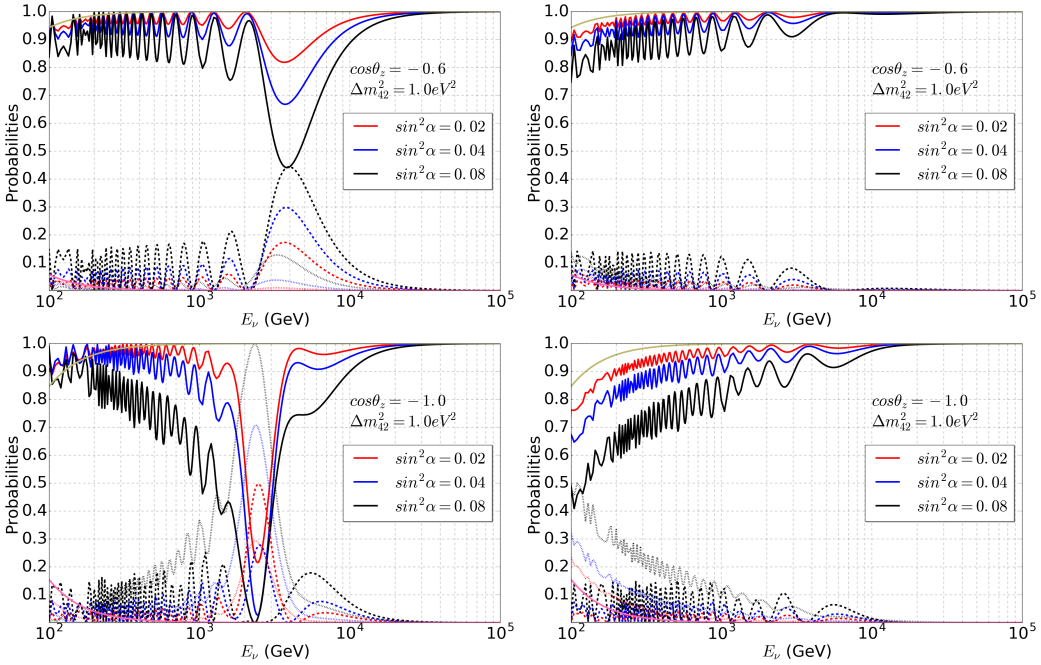

Figure 1: Oscillation probabilities for $\bar{\nu}_\mu$ (left panels) and ν_μ (right panels) for the mass-mixing scheme. The solid, dashed and dotted lines correspond to $P_{\mu\mu}$, $P_{\mu s}$ and $P_{\mu\tau}$ probabilities, respectively. The green and pink thin lines correspond to $P_{\mu\mu}$ and $P_{\mu\tau}$ probabilities, respectively, without any sterile neutrino mixing. Figure adapted from [20].

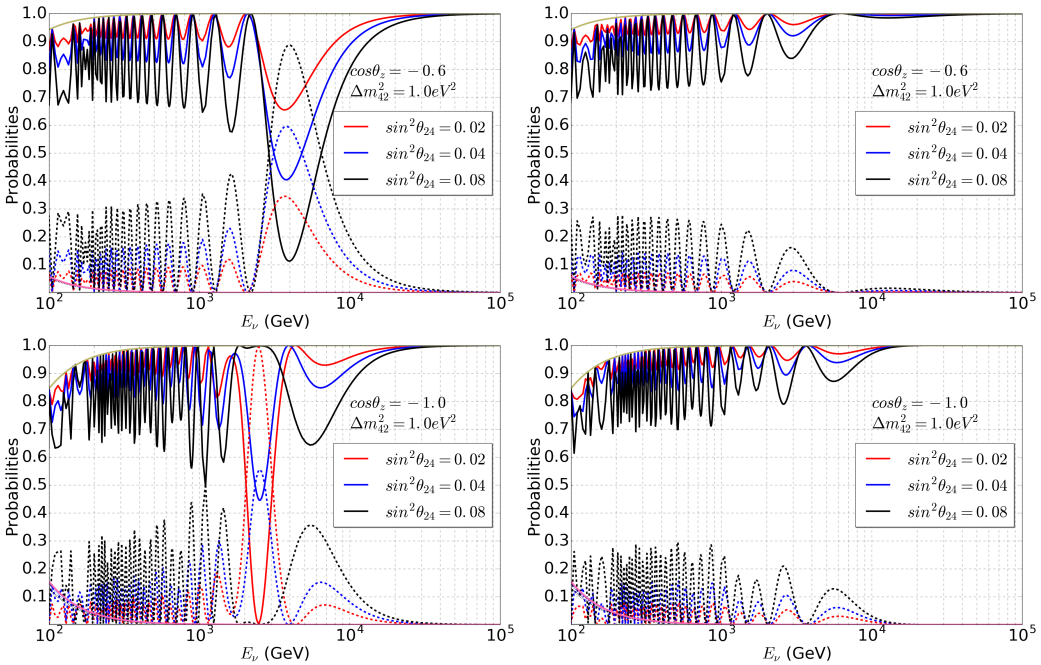

Figure 2: Same as figure 1 but for the flavor-mixing scheme. Figure adapted from [20].

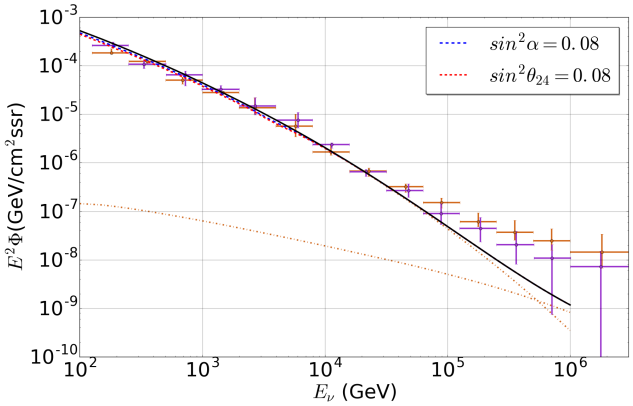

Figure 3: Atmospheric $\bar{\nu}_\mu + \nu_\mu$ flux data [30] and models, averaged over the zenith-angle range $(86^\circ - 180^\circ)$. The model consists of a conventional (orange dotted line [30]) and a prompt (orange dot-dashed line [21]) components, before any oscillation. The black solid line is the total without ν_s mixing and the blue-dashed (red-dashed) line is the total with ν_s mixing for the mass-mixing (flavor-mixing) scheme. Figure adapted from [20].

dashed lines. The data points are measurements by IceCube 79-string (magenta data points) and 86-string (orange data points) configurations [30].

The IceCube Collaboration has searched for sterile neutrinos using its IC86 data set of 20,145 well-reconstructed up going muon neutrino events, detected over a live time of 343.7 days (2011-2012) [12]. We use the same dataset, which is publicly available[1], in our study. The public data release also provides detector response arrays and conventional atmospheric flux models. These data arrays have the form: $T(E_\nu, \cos\theta_z, E_\mu)$, where E_ν is the primary neutrino energy, E_μ is the secondary muon energy and $\cos\theta_z$ is the muon direction.

We compare the IceCube data with simulated events with and without sterile neutrino mixing. We use the "nominal" detector response in order to calculate the number of expected events as

$$N(\cos\theta_z, E_\mu) = \sum_{(E_\nu)_{\rm bins}} T(E_\nu, \cos\theta_z, E_\mu)\bar{\phi}(E_\nu, \cos\theta_z)\,, \tag{3.2}$$

where the sum is over the neutrino energy bins. $\bar{\phi}(\cos\theta_z, E_\nu)$ is the average flux at the detector, for the same energy and zenith-angle bins as the data. We plot an example of the simulated event distributions in the zenith angle bins (left panel) and reconstructed muon energy bins (right panel), together with the IceCube data points in figure 4. In this example we have used the mass-mixing scheme to simulate events. To illustrate the effect of of the prompt component of the atmospheric neutrino flux, we have plotted the histograms with (labeled C+P) and without (labeled C) the prompt component of the flux. The effect of prompt flux component is evident at energies $\gtrsim 5 \times 10^3$ GeV (right panel) as it increases the number of simulated events.

4. Statistical analysis and constraints on the ν_s mixing parameters

In order to constrain the sterile neutrino mixing parameters we perform a detailed χ^2 analysis

[1] *http://icecube.wisc.edu/science/data/IC86-sterile-neutrino*

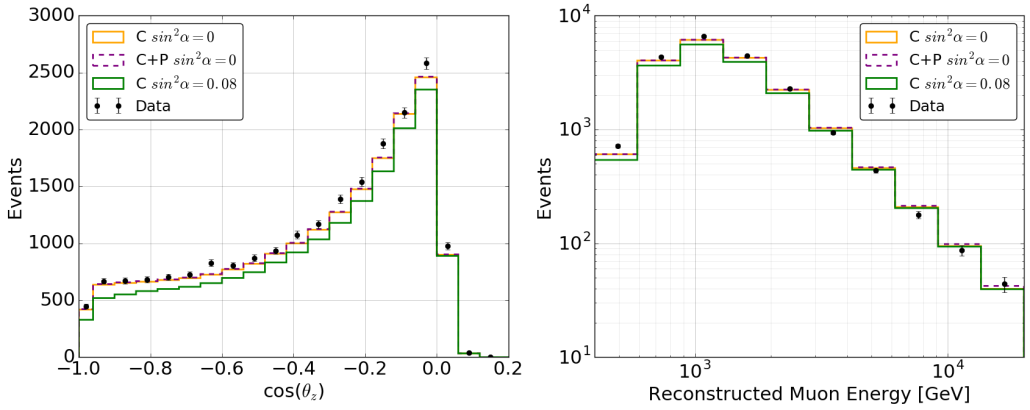

Figure 4: Comparisons of the IC86 data [12] and simulated events, using the conventional flux only (labeled C); conventional and prompt fluxes (labeled C+P), as well as without (labeled $sin^2\alpha = 0$) and with (labeled $sin^2\alpha = 0.08$) the ν_s mixing. Figure adapted from [20].

using the IC86 data and simulated events, with uncertainties in both the data and model. Following [18] we write the χ^2 function as

$$\chi^2(\sin^2\theta^*, \Delta m^2_{42}; \hat{\beta}) = \sum_{i,j} \frac{[(N_{ij})_{\rm exp} - \beta_0\beta_2[1+\beta_1(0.56+(\cos\theta_z)_i)](N_{ij})_{\rm mod}]^2}{(\sigma^2_{ij})_{\rm stat} + (\sigma^2_{ij})_{\rm syst}} + \frac{(1-\beta_0)^2}{\gamma_0^2} + \frac{\beta_1^2}{\gamma_1^2} + \frac{(1-\beta_2)^2}{\gamma_2^2} + \frac{\beta_3^2}{\gamma_3^2}\,, \tag{4.1}$$

where $\theta^* = \alpha$ or θ_{24}, depending on the ν_s mixing scheme. The parameters $\hat{\beta}$ correspond to the uncertainties of the atmospheric neutrino flux normalization (β_0); zenith dependence tilt (β_1); muon to electron neutrino ratio (β_2); and power-law index of the conventional flux (β_3). The IC86 data and simulated data are denoted by $(N_{ij})_{\rm exp}$ and $(N_{ij})_{\rm mod}$, respectively, with the i-th and j-th indices referring to the $\cos\theta_z$ and E_μ bins, respectively. The uncertainties on the $\hat{\beta}$ parameters we used for the calculation are: $\gamma_0 = 0.2$, $\gamma_1 = 0.04$, $\gamma_2 = 0.05$ and $\gamma_3 = 0.1$. For statistical uncertainty we use $(\sigma_{ij})^2_{\rm stat} = (N_{ij})_{\rm exp}$ and the uncorrelated systematic error $(\sigma_{ij})^2_{\rm syst} = f^2(N^2_{ij})_{\rm exp}$. The parameter f quantifies the detector precision. We use $f = 5\%$ and 10% in our analysis.

Figure 5 shows the constraints we obtain on the sterile neutrino mixing parameters: Δm^2_{42} and $\sin^2\theta_{24}$. The top panels are for the mass-mixing scheme, using $\sin^2\theta_{24} = \sin^2\alpha/(2-\sin^2\alpha)$ for conversion of the angle, and the bottom panels are for the flavor-mixing scheme. The exclusion regions are to the right of the black solid curves according to our analysis using the conventional atmospheric flux only. The red dashed lines correspond to the same but using both the conventional and prompt fluxes. The flavor-mixing scheme gives less tighter constraints because $2\sin^2\theta_{24} \approx \sin^2\alpha$, for small values of $\sin^2\alpha$. The exclusion regions begin to be less restrictive for $\Delta m^2_{42} \gtrsim 1$ eV^2, when taking into account the prompt atmospheric flux contribution as the number of events increases at higher energies which compensates some of the los events due to ν_s mixing. This change is greater with higher Δm^2_{42} and for smaller significance cases. Therefore the prompt-type flux contribution is important for $\Delta m^2_{42} \gtrsim 10$ eV^2 and $\sin^2\theta_{24} \lesssim 0.01$.

We exclude at $\gtrsim 3\sigma$ CL the 3σ allowed regions from the combined appearance experiments

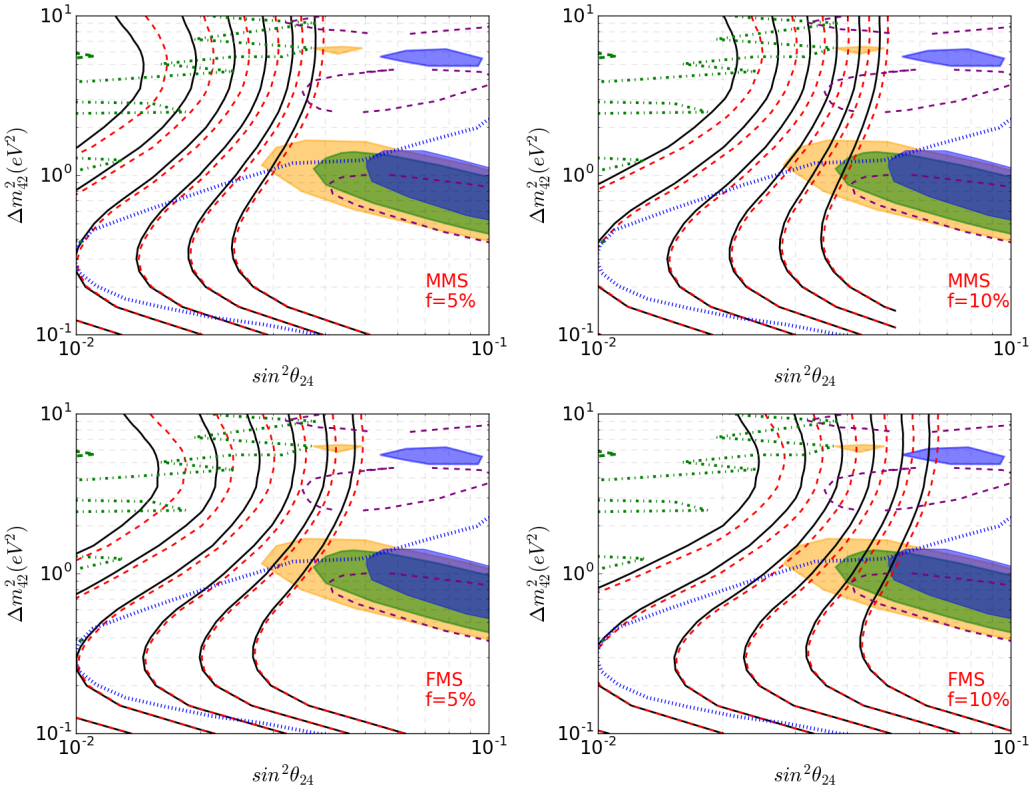

Figure 5: Constraints on the ν_s mixing parameters Δm^2_{42} and $\sin^2\theta_{24}$ at 1σ to 6σ CL from the left to right. The black solid (red dashed) lines correspond to the constraints using the conventional (prompt and conventional) atmospheric flux. The top (bottom) panels represent the constraints in the mass- (flavor-) mixing scheme. Also shown are IceCube constraint (blue dotted lines) at 99% CL [12] as well as the latest MiniBooNE 3σ allowed regions (purple dashed contours) [13]. See [20] for more details. Figure adapted from [20].

(orange shaded areas) in case of the flavor-mixing scheme with $f = 10\%$. The exlusion is at $\gtrsim 4\sigma$ CL in the case of mass-mixing scheme. We exclude at $\gtrsim 2\sigma$ CL the latest 3σ allowed regions from the MiniBooNE appearance results [13], in both the mixing schemes. Some small regions are allowed at the 3σ CL, however, when the prompt flux component is included (Fig. 5 bottom right panel) in the flavor-mixing scheme.

References

[1] A. Aguilar-Arevalo *et al.* [LSND Collaboration], Phys. Rev. D **64**, 112007 (2001) [hep-ex/0104049].

[2] A. A. Aguilar-Arevalo *et al.* [MiniBooNE Collaboration], Phys. Rev. Lett. **105**, 181801 (2010) [arXiv:1007.1150 [hep-ex]]

[3] G. Mention, M. Fechner, T. Lasserre, T. A. Mueller, D. Lhuillier, M. Cribier and A. Letourneau, Phys. Rev. D **83**, 073006 (2011) [arXiv:1101.2755 [hep-ex]].

[4] T. A. Mueller *et al.*, Phys. Rev. C **83**, 054615 (2011) [arXiv:1101.2663 [hep-ex]].

[5] J. N. Abdurashitov *et al.*, Phys. Rev. C **73**, 045805 (2006) [nucl-ex/0512041].

[6] Y. J. Ko *et al.* [NEOS Collaboration], Phys. Rev. Lett. **118**, no. 12, 121802 (2017) [arXiv:1610.05134 [hep-ex]].

[7] P. Adamson *et al.* [Daya Bay and MINOS Collaborations], Phys. Rev. Lett. **117**, no. 15, 151801 (2016) Addendum: [Phys. Rev. Lett. **117**, no. 20, 209901 (2016)] [arXiv:1607.01177 [hep-ex]].

[8] P. Adamson *et al.* [MINOS Collaboration], Phys. Rev. Lett. **117**, no. 15, 151803 (2016) [arXiv:1607.01176 [hep-ex]].

[9] P. Adamson *et al.* [MINOS+ Collaboration], Phys. Rev. Lett. **122**, no. 9, 091803 (2019) [arXiv:1710.06488 [hep-ex]].

[10] N. Agafonova *et al.* [OPERA Collaboration], JHEP **1806**, 151 (2018) [arXiv:1803.11400 [hep-ex]].

[11] M. G. Aartsen *et al.* [IceCube Collaboration], Phys. Rev. D **95**, no. 11, 112002 (2017) [arXiv:1702.05160 [hep-ex]].

[12] M. G. Aartsen *et al.* [IceCube Collaboration], Phys. Rev. Lett. **117**, no. 7, 071801 (2016) [arXiv:1605.01990 [hep-ex]].

[13] A. A. Aguilar-Arevalo *et al.* [MiniBooNE Collaboration], Phys. Rev. Lett. **121**, no. 22, 221801 (2018) [arXiv:1805.12028 [hep-ex]].

[14] H. Nunokawa, O. L. G. Peres and R. Zukanovich Funchal, Phys. Lett. B **562**, 279 (2003) [hep-ph/0302039].

[15] S. Choubey, JHEP **0712**, 014 (2007) [arXiv:0709.1937 [hep-ph]].

[16] S. Razzaque and A. Y. Smirnov, JHEP **1107**, 084 (2011) [arXiv:1104.1390 [hep-ph]].

[17] A. Esmaili, F. Halzen and O. L. G. Peres, JCAP **1211**, 041 (2012) [arXiv:1206.6903 [hep-ph]].

[18] A. Esmaili and A. Y. Smirnov, JHEP **1312**, 014 (2013) [arXiv:1307.6824 [hep-ph]].

[19] M. Lindner, W. Rodejohann and X. J. Xu, JHEP **1601**, 124 (2016) [arXiv:1510.00666 [hep-ph]].

[20] L. S. Miranda and S. Razzaque, JHEP **1903**, 203 (2019) [arXiv:1812.00831 [hep-ph]].

[21] R. Enberg, M. H. Reno and I. Sarcevic, Phys. Rev. D **78**, 043005 (2008) [arXiv:0806.0418 [hep-ph]].

[22] M. A. Acero *et al.* [NOvA Collaboration], Phys. Rev. D **98**, 032012 (2018) [arXiv:1806.00096 [hep-ex]].

[23] K. Abe *et al.* [T2K Collaboration], Phys. Rev. D **96**, no. 9, 092006 (2017) Erratum: [Phys. Rev. D **98**, no. 1, 019902 (2018)] [arXiv:1707.01048 [hep-ex]].

[24] M. G. Aartsen *et al.* [IceCube Collaboration], Phys. Rev. Lett. **120**, no. 7, 071801 (2018) [arXiv:1707.07081 [hep-ex]].

[25] A. M. Dziewinski and D. L. Anderson, Phys. Earth Planet Interiors **25**, 297 (1981)

[26] G. D. Barr, T. K. Gaisser, P. Lipari, S. Robbins and T. Stanev, Phys. Rev. D **70**, 023006 (2004) [astro-ph/0403630].

[27] M. Honda, T. Kajita, K. Kasahara, S. Midorikawa and T. Sanuki, Phys. Rev. D **75**, 043006 (2007) [astro-ph/0611418].

[28] T. K. Gaisser, Astropart. Phys. **35**, 801 (2012) [arXiv:1111.6675 [astro-ph.HE]].

[29] M. G. Aartsen *et al.* [IceCube Collaboration], Phys. Rev. D **89**, no. 6, 062007 (2014) [arXiv:1311.7048 [astro-ph.HE]].

[30] M. G. Aartsen *et al.* [IceCube Collaboration], Eur. Phys. J. C **77**, no. 10, 692 (2017) [arXiv:1705.07780 [astro-ph.HE]].